JACS
JOURNAL OF THE AMERICAN CHEMICAL SOCIETY
Article
pubs.acs.org/JACS

Photoexcited Surface Frustrated Lewis Pairs for Heterogeneous Photocatalytic CO_2 Reduction

Kulbir Kaur Ghuman,[†] Laura B. Hoch,[‡] Paul Szymanski,[§] Joel Y. Y. Loh,[⊥] Nazir P. Kherani,[⊥,†] Mostafa A. El-Sayed,[§] Geoffrey A. Ozin,[*,‡] and Chandra Veer Singh[*,†]

[†]Department of Materials Science and Engineering, University of Toronto, 184 College Street, Suite 140, Toronto, Ontario M5S 3E4, Canada

[‡]Department of Chemistry, University of Toronto, 80 St. George Street, Rm 326, Toronto, Ontario M5S 3E4, Canada

[§]Laser Dynamics Laboratory, School of Chemistry and Biochemistry, Georgia Institute of Technology, 901 Atlantic Drive, Atlanta, Georgia 30332-0400, United States

[⊥]The Edward S. Rogers Sr. Department of Electrical and Computer Engineering, University of Toronto, 10 King's College Road, Toronto, Ontario M5S 3G4, Canada

Supporting Information

ABSTRACT: In this study we investigated, theoretically and experimentally, the unique photoactive behavior of pristine and defected indium oxide surfaces providing fundamental insights into their excited state properties as well as an explanation for the experimentally observed enhanced activity of defected indium oxide surfaces for the gas-phase reverse water gas shift reaction, $CO_2 + H_2 + h\nu \rightarrow CO + H_2O$ in the light compared to the dark. To this end, a detailed excited-state study of pristine and defected forms of indium oxide (In_2O_3, In_2O_{3-x}, $In_2O_3(OH)_y$ and $In_2O_{3-x}(OH)_y$) surfaces was performed using time dependent density functional theory (TDDFT) calculations, the results of which were supported experimentally by transient absorption spectroscopy and photoconductivity measurements. It was found that the surface frustrated Lewis pairs (FLPs) created by a Lewis acidic coordinately unsaturated surface indium site proximal to an oxygen vacancy and a Lewis basic surface hydroxide site in $In_2O_{3-x}(OH)_y$ become more acidic and basic and hence more active in the ES compared to the GS. This provides a theoretical mechanism responsible for the enhanced activity and reduced activation energy of the photochemical reverse water gas shift reaction observed experimentally for $In_2O_{3-x}(OH)_y$ compared to the thermochemical reaction. This fundamental insight into the role of photoexcited surface FLPs for catalytic CO_2 reduction could lead to improved photocatalysts for solar fuel production.

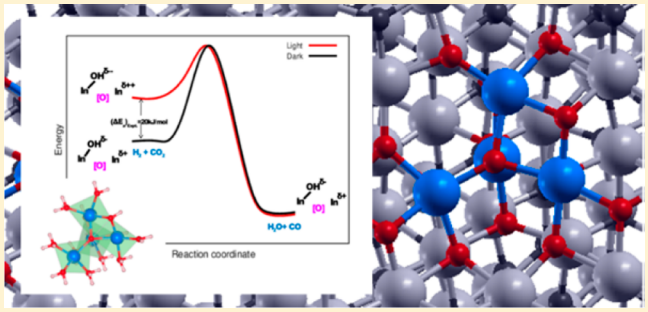

INTRODUCTION

Despite its relatively high cost, indium oxide, In_2O_3, is widely used as a substrate in a variety of applications, such as flat panel displays, solar cells, electrochromic windows, light emitting diodes, gas sensors and catalysis due to its favorable optical, electronic and surface properties.[1−4] In this context, In_2O_3 has also captured attention as a photocatalytic material.[5−9] Although it is understood that these applications inherently utilize the unique photochemical behavior of In_2O_3, to the best of our knowledge, very little is known about its excited-state (ES) physicochemical properties.

Our recent work[10] on indium oxide demonstrated that intentionally engineered surface defects can activate it for the photocatalytic hydrogenation of CO_2 to CO. Specifically, the gas-phase, light-assisted reduction of CO_2 using a defected form of indium oxide denoted $In_2O_{3-x}(OH)_y$, showed a conversion rate of 150 μmol·g^{-1}·hour^{-1}. Especially noteworthy, this rate was found to be four times higher in the presence of light compared to the dark. In addition, kinetic studies demonstrated that the activation energy was reduced by 20 kJ·mol^{-1} in the presence of light. However, the reason for this dramatic reduction in the energy barrier for CO_2 reduction in the light compared to the dark remained a mystery.

The concept of surface frustrated Lewis pairs (FLPs) emerged from this work providing a unique insight into the mechanism that could be responsible for CO_2 reduction in the ground state (GS). In particular, we demonstrated that only at specific surface sites containing adjacent Lewis basic In−OH groups and Lewis acidic, coordinatively unsaturated In atoms (created by surface oxygen vacancies) could CO_2 dissociate to release CO. Previously, the FLP concept was known only for homogeneous molecular-based chemistry and catalysts, and has been mainly utilized as a strategy that enables main group

Received: September 28, 2015
Published: January 13, 2016

DOI: 10.1021/jacs.5b10179
J. Am. Chem. Soc. 2016, 138, 1206−1214

compounds to activate small molecules.[11−13] Nonetheless, the role of surface FLPs in ES chemistry and catalysis remains unknown. This motivated us to study pristine and defected In_2O_3 surfaces in the presence of light compared to the dark to gain an insight into the role surface hydroxide and surface oxygen vacancy defects play in the GS and ES reverse water gas shift reaction.

To this end, we have clarified the nature of the ES in pristine In_2O_3 and defected In_2O_{3-x}, $In_2O_3(OH)_y$ and $In_2O_{3-x}(OH)_y$ surfaces for the first time by using the TDDFT method. Furthermore, to validate the conclusions drawn from the TDDFT results, we also conducted transient absorption (TA) spectroscopy measurements on photocatalytically active $In_2O_{3-x}(OH)_y$ samples, containing coordinately unsaturated indium, oxygen vacancy and hydroxide surface defect sites. The strong correlation observed between sub-bandgap defect states predicted by the TDDFT model with the defect transitions detected in the experimental TA spectra, provides compelling support for our theoretical results. We further validated the TDDFT results using wavelength dependent photoconductivity measurements, which clearly illustrate a photoresponse in experimental $In_2O_{3-x}(OH)_y$ films, even when illuminated with light energy well below the fundamental band gap. Using charge transition density analysis, this study not only analyzed and compared the ES properties of pristine and defected In_2O_3 surfaces but also showed the importance of ES surface FLP active sites in gas-phase light-assisted heterogeneous catalytic reduction of CO_2 to CO.

MATERIALS AND METHODS

Computational Methods. To analyze the excited states of pristine and defected forms of indium oxide, the NWChem package[14] within linear response time-dependent density functional theory (LR-TDDFT) was used. LR-TDDFT in combination with appropriate exchange correlation functionals has become an attractive method for reliable excited state calculations involving single excitations in a wide range of materials.[15,16] In this work, the B3LYP exchange correlation potential was used which has been shown to perform well for the In_xO_y system[17] with the split-valence double- zeta 3-21G basis set. With this description, we have a total of 365 and 314 basis functions for the pristine bulk and surface In_2O_3 cluster, respectively. In these calculations, no effective core potential was used, hence all electrons (e.g., 324 electrons for the 50 atom cluster of pristine In_2O_3, Figure 1(a)) actively participated in the configurational space. The clusters were fully geometry optimized using quasi-newton algorithm with the convergence criterion of 10^{-8} Hartree (1 Hartee = 13.6 eV) for the energy and 10^{-6} Hartree/Bohr for its gradient. During optimization, all of the interior atoms were allowed to move, while all of the pseudohydrogen saturators were kept fixed. To ensure the global minima of each cluster, frequency calculations were conducted for the optimized geometries which yielded zero imaginary frequencies. Figures 1a, 1b, 1c and 1d show the optimized cluster models of the pristine In_2O_3, In_2O_{3-x}, $In_2O_3(OH)_y$ and $In_2O_{3-x}(OH)_y$ surfaces, respectively. In order to understand the role of defects, the ground-state geometries of the clusters representing pristine In_2O_3 and defected In_2O_{3-x}, $In_2O_3(OH)_y$ and $In_2O_{3-x}(OH)_y$ surfaces were used for the TDDFT calculations in this study.

Materials Synthesis. The synthesis of the $In_2O_{3-x}(OH)_y$ photocatalytic nanocrystals has been described in detail elsewhere.[18] Briefly, an amorphous indium hydroxide precursor was synthesized by dissolving indium(III) chloride (3.6 g, 16.2 mmol, Sigma-Aldrich, 98%) in a 3:1 solution of anhydrous ethanol (54 mL, Commercial Alcohols) and deionized, nanopure water (18 mL, resistivity 18.2 MΩ cm). A separate solution of 3:1 mixture of ethanol (54 mL) and ammonium hydroxide (18 mL, Caledon, 28−30% adjusted to 25 wt % with deionized water) was rapidly added, resulting in the immediate formation of a white precipitate. The resulting suspension was immediately immersed in a preheated oil bath at 80 °C and stirred at a high rate for 10 min. The precipitate was then separated via centrifugation and washed 3 times with deionized water. Subsequently, the precipitate was sonicated between washings to ensure adequate removal of any trapped impurities and then dried overnight at 80 °C in a vacuum oven. The dried precursor powder was finely ground with a mortar and pestle, and calcined for 3 h in air at 250 °C.

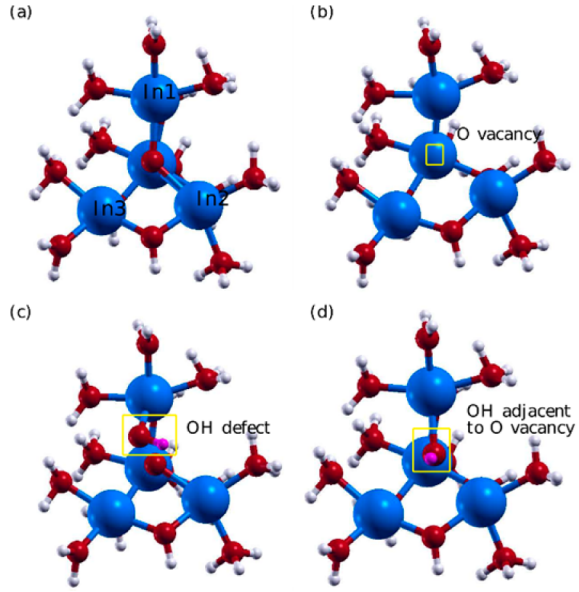

Figure 1. Optimized geometric structures of (a) pristine In_2O_3, (b) In_2O_{3-x}, (c) $In_2O_3(OH)_y$ and (d) $In_2O_{3-x}(OH)_y$ surfaces in the ground state. Indium atoms are represented in blue, hydrogen saturators in white, oxygen atoms in red and the hydrogen atom of the surface OH group in pink.

Materials Characterization. Powder X-ray diffraction (PXRD) was performed on a Bruker D2-Phaser X-ray diffractometer, using Cu Kα radiation at 30 kV. Sample morphology was determined using a JEOL-2010 high resolution transmission electron microscope (HR-TEM). Diffuse reflectance of the sample was measured using a Lambda 1050 UV/vis/NIR spectrometer from PerkinElmer and an integrating sphere with a diameter of 150 mm. The diffuse reflectance spectrum was then fitted with a modified Kubelka−Munk function[19] to determine the optical band gap of each sample. Specifically, $(F(R)*h\nu)^n$ is plotted as a function of photon energy where $F(R) = (1 - R)^2/2R$; R is the diffuse reflectance of the sample and n was set to 3/2 in accordance with the direct forbidden band gap of In_2O_3. The linear portion of the plot was extrapolated and its intercept with the abscissa provided the band gap estimate.

Transient absorption measurements were carried out with a Helios UV−visible spectrometer (Ultrafast Systems). A pump wavelength of 318 nm was chosen to excite the sample above the optical-band gap. The pump light was obtained from the fourth harmonic of the signal from a Coherent OPerA Solo optical parametric amplifier which was pumped by a Coherent Libra regeneratively amplified Ti:sapphire laser (809 nm, 50 fs pulses, 1 kHz repetition rate). A broadband probe beam was produced by focusing a small fraction of the fundamental wavelength into a sapphire or CaF_2 crystal. Both pump and probe were focused and overlapped on the surface of the sample-coated quartz substrate. The transmitted probe light was used to determine the transient absorption by focusing it into a fiber-coupled Si array detector with a detection range of 300−907 nm. Scattered pump light was blocked by a long-pass filter placed before the detector. A rotating mechanical chopper blocked every other pump pulse with the difference between two consecutive spectra—one with the pump beam, and one without—yielding the TA signal $\Delta A(t)$, where t is the time delay between pump and probe pulses.

DOI: 10.1021/jacs.5b10179
J. Am. Chem. Soc. 2016, 138, 1206−1214

The spot size of the pump beam incident on the sample was used to determine the fluence, or energy per laser pulse divided by the irradiated area. For one-photon absorption, the number of absorbed photons is proportional to the incident fluence. The spatial profile of the laser beam spot on the sample surface was approximately a two-dimensional Gaussian. The radius of the beam is defined as the length over which the intensity falls from the maximum to $1/e^2$ times the maximum. This radius was measured by the knife-edge method, in which a beam block with a straight edge (in this case, a razor blade) is translated through the laser spot and the power is recorded as a function of the beam block position.[20] The razor blade was placed in the Helios sample holder and translated by a Newport NSA12 motorized actuator, with the power measured by a calibrated Si photodiode optical power sensor (Newport 818-UV).

An approximately 50 μm thick film of close packed $In_2O_{3-x}(OH)_y$ nanoparticles was layered with an array of 1 mm by 1 mm silver electrodes of 250 μm spacing. An external quantum efficiency (EQE) measurement setup comprising a Keithley 2440 source meter, Spectra Product CM110 monochromator, Hg/Xe 200W lamp, Princeton Model 5210 lock in amplifier, beam splitter and chopper was used to conduct a 4 point probe I−V measurement over a 650 to 420 nm incident wavelength spectral range from the higher wavelengths to lower wavelengths in order to prevent persistent photoconductivity at the main absorption edge from carrying over to the higher wavelengths. The conductance value at each wavelength point was taken after a 10 min illumination to allow any significant photocurrent value change to be detected. The measured photocurrent was normalized over the incident power to determine the EQE. To prove that photoconductivity is present at the higher wavelength regime, we took photoconductance measurements at several monochromatic wavelengths (380, 420, 450, 480, 520, 560 and 632 nm He−Ne 1 mW laser) over time with illumination on and subsequently off. No change in conductivity was detected with a 50 mW 913 nm (1.35 eV) laser.

RESULTS AND DISCUSSION

Development and Validation of Cluster Models. Since the detailed excited state computations on a periodic (slab) model of In_2O_3 (111) surface would be computationally prohibitive, equivalent saturated cluster models were developed.[21−24] The covalent embedding procedure,[21,22] where cluster models are terminated with suitably chosen pseudohydrogen saturators, is used to model the surface of pristine defect-free In_2O_3 (In_2O_3), shown in Figure 1a, and with only oxygen vacancy (In_2O_{3-x}), only hydroxide ($In_2O_3(OH)_y$) and both O vacancy and hydroxide ($In_2O_{3-x}(OH)_y$) defects, shown in Figure 1b, Figure 1c and Figure 1d, respectively. Previously, this approach has been effectively used to characterize and study the structural, electronic and optical properties of a wide variety of surfaces such as TiO_2(110), ZnO(1000), CuCl(111) and V_2O_5(010).[23,15,25−27] The (111) termination for the In_2O_3 surface was chosen since it is the most favored termination thermodynamically[28] and also corresponds well with surfaces observed in the experimental samples, as discussed in our previous study.[10]

All indium oxide clusters were terminated using pseudohydrogen saturators having appropriately chosen classical point charges at the same coordinates (see details in the Supporting Information). These models were further tested and validated by probing the convergence of the optical properties with respect to the size of the cluster by studying absorption spectra of 120 atoms ($In_9O_{33}H1_{78}$), 80 atoms ($In_5O_{21}H1_{54}$) and 64 atoms ($In_4O_{17}H1_{43}$) bulk-like clusters, Figure S3). Almost no dependence of the optical band gap on the cluster size was observed. Moreover, since the bulk and surface clusters have different saturation of the bordering In and O atoms, by comparing the absorption spectra of the bulk cluster model with the surface cluster model (Figure S1a and S1b) we are probing the convergence of optical properties with the method of saturation. Furthermore, the optical properties of the surface cluster were also found to be in good agreement with the experimental data obtained for $In_2O_{3-x}(OH)_y$ samples (Figure S1d). This indicates that the accuracy of the local description of the potential is more important than the inclusion of long-range effects and that these saturated cluster models can be used to correctly mimic the properties of pristine and defected forms of In_2O_3.

Structural Changes during Light Activation for Pristine and Defected Surfaces. The geometric structures for all four surfaces, In_2O_3, In_2O_{3-x}, $In_2O_3(OH)$, and $In_2O_{3-x}(OH)_y$, were fully optimized for the GS by the DFT method and for the ES by the TDDFT method. Some salient bond lengths and bond angles for these surface clusters in the GS and ES are listed in Table S1 in the Supporting Information. Structural analysis for the pristine surface cluster shows a slight geometric contraction of the surface structure in the presence of light. In contrast, the surface containing only an O vacancy defect shows a slight expansion in the ES. However, when a surface O is replaced with OH, the system behaves similarly to the pristine In_2O_3 surface, and shows contraction in the presence of light. Thus, adding an extra H (of OH) does not seem to disturb the structure as much as when an O is taken out of the pristine surface. Interestingly, the structure of the surface having both O vacancy and OH defects is not significantly influenced by light. All In···In distances remain almost unchanged in the ES for the $In_2O_{3-x}(OH)_y$ structure; while the bond length of the hydroxyl group is slightly decreased from 1.015 to 0.998 Å and the neighboring In−OH distance is lengthened by 0.004 Å in the ES. Although small, these spatial changes brought by defect interactions with light could be associated with the change in reaction mechanism from GS to ES, resulting in a lower activation barrier for CO_2 reduction in the light compared to the dark, as discussed in the following sections.

Absorption Spectra. To investigate the role of light on optical properties, UV−visible absorption spectra were computed for pristine In_2O_3 and defected In_2O_{3-x}, $In_2O_3(OH)_y$, and $In_2O_{3-x}(OH)_y$ surfaces as shown in Figure 2, where the vertical lines denote the corresponding excitation energies and oscillator strengths. The oscillator strengths were determined to express the intensities of transitions between two states. The calculated energies and oscillator strengths of the lowest-lying transitions for all the surfaces are tabulated in Table 1.

The low-energy absorption band for the pristine In_2O_3 surface (Figure 2a) mainly consists of two transitions, viz. the S0 → S1 and S0 → S2 transitions at 3.34 and 3.37 eV, respectively. The S1 and S2 states are nearly degenerate with the S0 → S1 transition, involving the promotion of an electron from the bonding highest-occupied molecular orbital (HOMO) into the lowest-unoccupied molecular orbital (LUMO); and, the S0 → S2 transition involving the promotion of an electron from the HOMO−1 into the LUMO. In these TDDFT calculations, the HOMO of the pristine In_2O_3 surface can be considered to correspond to the valence band maximum (VBM) of the material and the LUMO to correspond to the conduction band minimum (CBM). The main contribution to the absorption band for the pristine surface is due to the S0 →

DOI: 10.1021/jacs.5b10179
J. Am. Chem. Soc. 2016, 138, 1206−1214

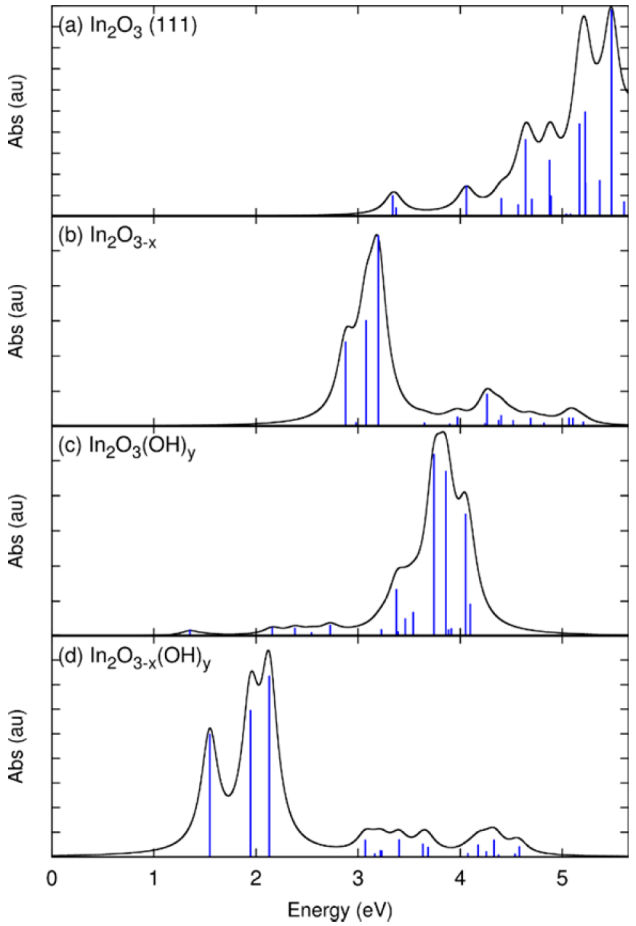

Figure 2. TDDFT-calculated absorption spectra for (a) pristine In_2O_3 and defected (b) In_2O_{3-x}, (c) $In_2O_3(OH)_y$ and (d) $In_2O_{3-x}(OH)_y$ surfaces. Vertical lines correspond to unbroadened excitation energies and oscillator strengths.

S16 transition at 5.48 eV with maximum oscillator strength of 0.109.

In contrast to the above, the surface containing only O vacancy defects (In_2O_{3-x}) shows a sharp peak with oscillator strength of 0.285 in the visible region (Figure 2b). Here, the absorption band mainly consists of three transitions: the S0 → S1, S0 → S2, and S0 → S3 transitions at 2.88, 2.98, and 3.08 eV, respectively. It is found that the first transition is mainly due to the promotion of an electron from HOMO to LUMO+1 and LUMO+2. The intense absorption associated with these first three transitions masks the contributions of the rest of the transitions, whose oscillator strengths are negligible. In contrast to the O vacancy only In_2O_{3-x} surface, the hydroxide only $In_2O_3(OH)_y$ surface shows no noticeable peaks in the visible region due to the presence of hydroxide groups (Figure 2c). In fact, the first nine excited states show negligible oscillator strengths for this surface, signifying that these transitions do not contribute to absorption spectra. The first noticeable absorption band for the $In_2O_3(OH)_y$ surface is due to the S0 → S10 transition at 3.37 eV (oscillator strength = 0.0134), which is similar to the first absorption band of pristine In_2O_3 surface. This might be due to the minimal distortion of the surface by substitution of O with OH. It is found that this transition is mainly due to promotion of electrons from HOMO−1 to LUMO+1. Thus, unlike other surfaces studied herein, the $In_2O_3(OH)_y$ surface shows no significant contribution to its first significant absorption band arising from charge transfer from HOMO to LUMO.

Table 1. TDDFT Results for the Five Lowest-Lying Excited Singlet States for Pristine In_2O_3 and Defected In_2O_{3-x}, $In_2O_3(OH)_y$ and $In_2O_{3-x}(OH)_y$ Surfaces: Excitation Energy (EE) (eV), Oscillator Strengths (OS) and the Dominant Orbital Transitions Contributions (dom. OT contr.)[a]

states	EE(eV)	OS	dom. OT contr.
		pristine (111) In_2O_3 surface	
S1	3.3384	0.01117	H → L (97%)
S2	3.7313	0.00490	H-1 → L (95.4%)
S3	4.0588	0.01632	H-2 → L (98.8%)
S4	4.4023	0.00974	H-3 → L (95.0%)
S5	4.5665	0.00646	H-1 → L+1 (77.3%)
		In_2O_{3-x} surface	
S1	2.8779	0.28504	H → L+1 (63.0%), H → L+2 (20.2%)
S2	2.9796	0.01482	H-1 → L (89.4%)
S3	3.0775	0.35535	H → L+2 (44.3%), H → L+1 (31.0%)
S4	3.1970	0.64017	H → L (62.3%)
S5	3.6487	0.01379	H-1 → L+1 (96.1%)
		$In_2O_3(OH)_y$ surface	
S1	1.3521	0.00188	H → L (51.6%), H-1 → L (36.9%)
S2	1.4792	0.00028	H-1 → L (58.8%), H → L (39.3%)
S3	1.5681	0.00016	H-2 → L (23.3%), H-5 → L (23.0%)
S4	2.1592	0.00260	H-4 → L (38.3%), H-5 → L (26.6%)
S5	2.3815	0.00249	H-2 → L (65.5%), H-3 → L (22.2%)
		$In_2O_{3-x}(OH)_y$ surface	
S1	1.5466	0.13342	H → L (100%)
S2	1.9463	0.15913	H → L+1 (99.0%)
S3	2.1288	0.19625	H → L+2 (99.6%)
S4	3.0700	0.01881	H → L+3 (92.4%)
S5	3.1638	0.00374	H → L+4 (93.0%)

[a]H, HOMO; L, LUMO.

In Figure 2d, the absorption spectra for $In_2O_{3-x}(OH)_y$ surface containing both O vacancy and OH by contrast shows three well-defined peaks at 1.55, 1.95, and 2.13 eV with oscillator strengths of 0.133, 0.159, and 0.196 due to the S0 → S1, S0 → S2, and S0 → S3 transitions, respectively. Further analysis reveals that these three transitions are due to the promotion of electrons from HOMO to LUMO, HOMO to LUMO+1, and HOMO to LUMO+2, respectively. The contributions of the rest of the transitions and their intensities are observed to be negligible.

It is important to note that in the experimental absorbance spectrum of $In_2O_{3-x}(OH)_y$ in Figure S1d, no peaks are visible in the region corresponding to energies less than 2.9 eV. This indicates that the primary optical transitions from the valence band maximum (VBM) to the conduction band minimum (CBM) for $In_2O_{3-x}(OH)_y$ can be described by the HOMO to LUMO transitions in the pristine In_2O_3 surface. However, the $In_2O_{3-x}(OH)_y$ cluster model containing both O vacancy and OH defects predicts HOMO to LUMO transitions to occur at energies of 1.55, 1.95, and 2.13 eV, which would fall within the fundamental band gap of In_2O_3. However, the creation of midgap states by the introduction of O vacancy and OH defects in indium oxide materials is consistent with other reports found in the literature[29,30] and in our previous work, we demonstrated the presence of both of these defects in our photocatalytically active $In_2O_{3-x}(OH)_y$ material.[10,18] The absence of visible light absorption in the experimental $In_2O_{3-x}(OH)_y$ spectrum is likely due to several factors. First, in our experimental $In_2O_{3-x}(OH)_y$

DOI: 10.1021/jacs.5b10179
J. Am. Chem. Soc. 2016, 138, 1206−1214

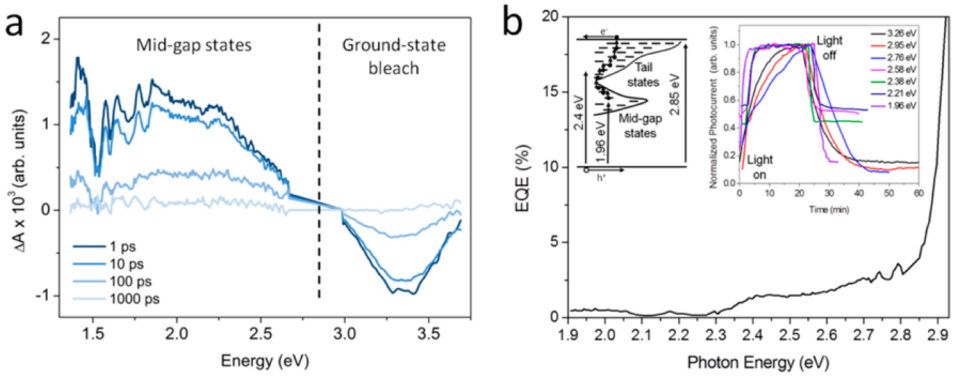

Figure 3. (a) Transient absorption spectra at different time delays between pump and probe pulses of the $In_2O_{3-x}(OH)_y$ samples excited with 318 nm light at an incident fluence of 0.124 mJ/cm^2 per pulse. All spectra are plotted as the difference from the original absorption spectrum, so a positive peak indicates increased absorption relative to the ground state, while a negative peak indicates decreased absorption. (b) External quantum efficiency (EQE) spectra from 1.9 to 2.9 eV with a long tail of photocurrent change at lower incident photon energies. The photocurrent rise edge corresponds with the absorption edge of 2.8 eV. Right Inset shows the normalized photocurrent rise, saturation and decay when monochromatic light is on and off. Left Inset shows a possible band diagram of overlapping tail and midgap states that enables photogeneration and thermal hopping at sub band gap illumination.

material the concentration of O vacancy and hydroxide defects is relatively small compared to the overall defect-free crystalline regions. Therefore, the defect-free absorption likely dominates, which could explain why our experimental absorption more closely resembles the pristine surface. Indeed Lei et al. have demonstrated the effect of O vacancy concentration on the absorption spectrum of indium oxide samples.[30]

Their results illustrate that only at high O vacancy concentration is a substantial visible absorption observed, while at low O vacancy concentration, the absorption spectrum more closely resemble the bulk absorption spectrum of indium oxide. Further, if optical transitions from these midgap states are short-lived, it would result in signal broadening, making it more difficult to detect by standard steady-state absorption spectroscopy,[31] particularly if the signal was small to begin with.

In order to confirm the existence of these proposed midgap states to further validate this model, we used transient absorption (TA) spectroscopy, which is a sensitive technique that uses a high-intensity laser excitation source and is able to detect very short-lived excited state transitions. In TA spectroscopy, an ultrafast, single-wavelength laser pump pulse is used to put the sample into an excited state by promoting electrons from the valence band to the conduction band, creating electron−hole pairs. These excited state charge carriers rapidly relax to the bottom of the conduction band or top of the valence band and can begin to populate midgap defect states, typically within <1 ps after light is absorbed.[32−34] This first laser pump pulse is then followed by a second broad band laser probe pulse, which measures the excited state absorption spectra of the sample at different time delays (1−1000 ps) after the initial excitation.

Figure 3 shows the TA spectra of the photoactive $In_2O_{3-x}(OH)_y$ nanocrystal sample at different time delays between pump and probe pulses. There are two distinct regions observed. The negative change in absorbance (ΔA) for wavelengths corresponding to energies above the band gap (>2.9 eV), relating to the ground-state absorption of the $In_2O_{3-x}(OH)_y$ nanocrystals, is called the ground-state bleach. This is associated with state-filling resulting from the initial excitation of the $In_2O_{3-x}(OH)_y$ nanocrystals from the ground state to the excited state. Because these spectra are plotted relative to the original absorption spectrum, this reduction in the number of charge carriers in the ground state due to the first laser pump pulse results in less absorption observed using the probe pulse, and therefore a negative ΔA signal. On the other hand, wavelengths corresponding to energies below the band gap (<2.9 eV) do not appear to contribute substantially to the ground state absorption. The positive ΔA in these regions of the spectra are therefore associated with secondary excitation of the already photoexcited charge carriers to higher energy states due to the probe pulse. This positive photoinduced ΔA depends on the number of photogenerated charge carriers present and the coupling efficiency between the initial and final states.[35−37] From the TA spectra it is apparent that a broad distribution of transitions are occurring that correspond to energies below the band gap of indium oxide. In TA studies of similar, ligand-free, defected metal oxides (e.g., TiO_2, ZnO), a positive ΔA in the visible region is typically assigned to transitions from electrons and holes populating midgap states created by surface and bulk defects.[33,38−42] O vacancy defects generally have been shown to behave as electron traps and give rise to TA signals around ∼1.8 eV,[33,39] while hydroxide groups are often considered to create hole traps that produce TA signals around ∼2.4 eV.[43] Signals in the near-infrared (>1.5 eV) are generally attributed to transitions from defect states, particularly surface oxygen vacancies, into the conduction band.[33,39−42] It should be noted that energy values of these TA optical transitions, which are the result of secondary excitation from pump−probe measurements, cannot be directly correlated to the direct HOMO to LUMO transitions in the computational models, however their presence, combined with literature precedent, provides compelling evidence for the presence of midgap defect states predicted by the theoretical $In_2O_{3-x}(OH)_y$ cluster model. Further it is apparent that contributions to the TA spectra from these midgap states is only significant within the first 1000 ps, indicating that charges populating these midgap states very rapidly relax back to the ground state, which would result in signal broadening, further helping to explain the absence of visible absorption in the steady-state absorption spectra.

In order to provide further evidence of the presence of optically active midgap defect states in our $In_2O_{3-x}(OH)_y$ sample, we conducted photoconductivity measurements. A film of the $In_2O_{3-x}(OH)_y$ nanoparticles was layered with silver

DOI: 10.1021/jacs.5b10179
J. Am. Chem. Soc. 2016, 138, 1206−1214

electrodes with a period spacing of 0.5 mm and 4 point probe measurements were conducted. As shown in Figure 3b, the EQE spectrum shows an appreciable tail of conductance from energy levels above ∼2.3 eV and an additional weak contribution around 1.9−2.0 eV. As illustrated in the inset of Figure 3b, this indicates that electrons with energies above 1.9 eV are excited from the valence band or populated defect states into a continuum of states within the band gap from where they are able to thermally hop to the conduction mobility edge. The slow photoconductivity change with time (right inset of Figure 3b) shows that photogenerated carriers undergo significant recombination and regeneration before reaching photosaturation; and when the light is turned off, trapped carriers in deep states are slow to relax.[44] It is possible that midgap states from 1.9−2.2 eV which overlap with the exponential band tail enable electron conduction (see left inset of Figure 3b) however the number of photogenerated carriers participating in conduction may be restricted by the percolation pathway giving rise to a weaker photoconductivity change than that measured for states from 2.3−2.7 eV. It is also possible that midgap states themselves provide a conduction pathway between nanoparticles.[45] While further investigation is required to determine the exact conductivity mechanisms, these measurements further support the existence of deep to midgap defect states in the $In_2O_{3-x}(OH)_y$ sample, corresponding well with what has been predicted theoretically.

Molecular Orbital and Transition Density Analysis. To analyze the charge transfer properties due to excitations for a complex system of the type described herein, the most commonly used method is analysis of the molecular orbitals (MOs) involved in the electronic transition. Based on the calculated electronic excitation energies, the photoexcitation is expected to electronically excite In_2O_3 to the S1 and S2, In_2O_{3-x} to S1, $In_2O_3(OH)_y$ to S10 and $In_2O_{3-x}(OH)_y$ to S1, S2 and S3 states. These first few excited states also possess considerable intensity in the visible range and are therefore analyzed further using MOs involved in these excitations. To explicitly illustrate the nature of the charge distribution associated with these excitations, we also computed the transition densities (TD) as described later in this section.

Figure 4a shows the dominant MO contributors for the S0 → S1 and S0 → S2 excitations of the pristine In_2O_3 surface. These lowest energy transitions are dominated by charge transfer excitation from the HOMO and HOMO−1, which are associated with surface O atoms, to the LUMO which are associated mainly with In atoms. It should be noted that this HOMO and LUMO character of the finite cluster model considered here is similar to that reported for the slab model[10,46] indicating that our model contains the necessary ingredients to capture the essential physics of this system. Further, the TD distribution for the pristine surface depicted in Figure 5a shows that almost all the In and O atoms of the cluster contribute to electron−hole pairs for the S1 excited state, indicating the nature of the delocalized charge contribution, where the O atoms act as donor and In atoms act as acceptors.

The calculated absorption spectrum (Figure 2b) showed intensities at lower energies for the surface with only O vacancy defects. The dominant MOs contributing to the first significant (S0 → S1) excitation responsible for this visible absorption are shown in Figure 4b. It can be seen that the S0 → S1 transition is dominated by charge transfer from the HOMO, which is mainly associated with excess charge on the surface due to the

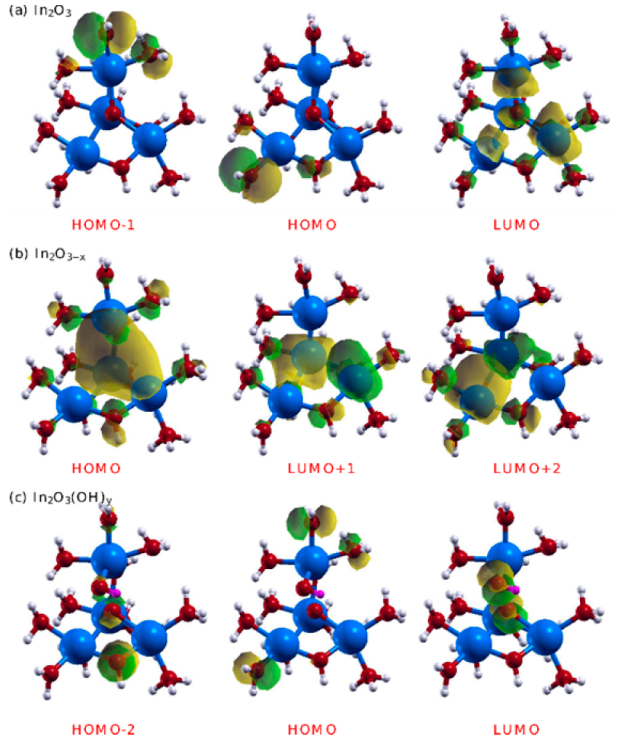

Figure 4. Molecular orbitals contributing to (a) S0 → S1 and S0 → S2 transitions of pristine In_2O_3, (b) S0 → S1 transition of defected In_2O_{3-x} and (c) S0 → S10 transition of defected $In_2O_3(OH)_y$ surfaces.

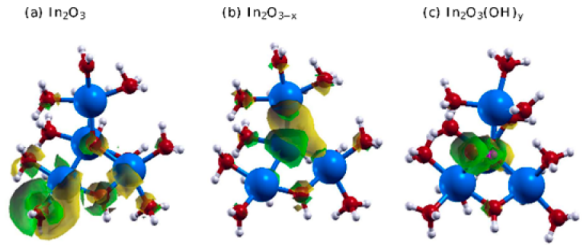

Figure 5. Representative transition densities for the (a) S1 excited state of pristine In_2O_3, (b) S1 excited state of defected In_2O_{3-x}, and (c) S10 excited state of defected $In_2O_3(OH)_y$ surfaces.

O vacancy, to the LUMO+1 and LUMO+2, which is delocalized mainly around the In sites. Further, the TD for the In_2O_{3-x} surface displayed in Figure 5b shows that the charge dynamics are much more localized around the O vacancy. Most of the charge accumulation and depletion occurs in the vicinity of the O vacancy and the In atoms bonded to it, with a smaller amount of charge accumulation reaching the more distant In atoms. This is in stark contrast to the excitation in the pristine In_2O_3 surface, which is far more delocalized.

As discussed earlier, the absorbance intensities of the first nine lowest energy excitations for the $In_2O_3(OH)_y$ surface are found to be negligible. The dominant MO contributions to the first five excitations are given in Table 1. In Figure 4c, we represent the charge transfer process for the S0 → S10 transition at 3.37 eV, which is found to be responsible for the first significant absorption band, Figure 2c. The S0 → S10 transition is dominated by charge transfer from HOMO and HOMO−2, delocalized over the p orbitals of the O atoms of the cluster, to LUMO, which is mainly localized over the p orbitals of the O of the OH group and the neighboring surface O atom. The TD of the $In_2O_3(OH)_y$ surface, Figure 5c, shows

DOI: 10.1021/jacs.5b10179
J. Am. Chem. Soc. 2016, 138, 1206−1214

that the electron−hole pairs associated with the first significant absorption band mainly exist on the O atom of the OH group and its neighboring O, indicating a localized charge distribution as in the case of In_2O_{3-x} surface.

Figure 6a, 6b, 6c display the MO contributors to the S0 → S1, S0 → S2, and S0 → S3 transitions of the $In_2O_{3-x}(OH)_y$

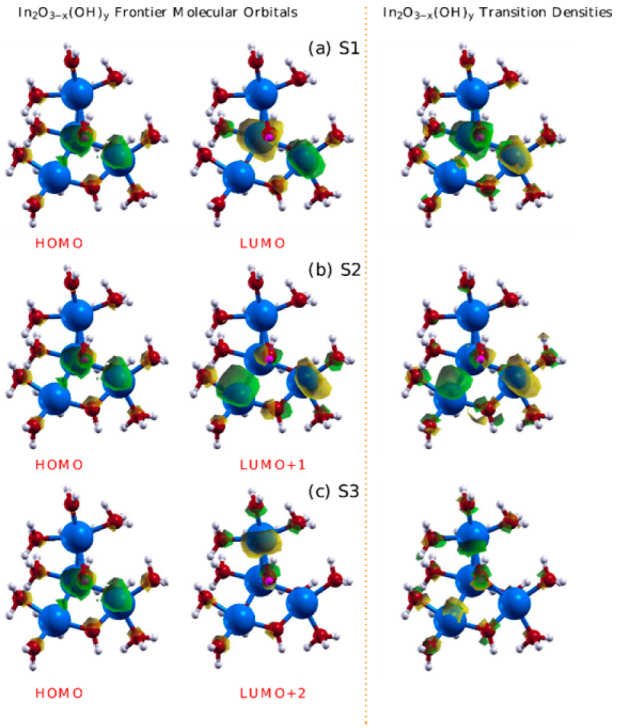

Figure 6. Visualization of the main contributing molecular orbitals and transition densities for (a) S1 (HOMO → LUMO) (b) S2 (HOMO → LUMO+1) and (c) S3 (HOMO → LUMO+2) excited states of the defected $In_2O_{3-x}(OH)_y$ surface.

surface, respectively. Table 1 shows that out of these three transitions, S0 → S3 transition has the maximum oscillator strength and therefore will be responsible for the overall charge distribution. The S0 → S1, S0 → S2 and S0 → S3 transitions are dominated by charge transfer excitation from HOMO to LUMO, HOMO to LUMO+1, and HOMO to LUMO+2, respectively. As shown in these figures, the HOMO of the $In_2O_{3-x}(OH)_y$ surface is mainly associated with s and p orbitals of the surface In atom (In2, Figure 1) with a small contribution from the s orbitals of the O atoms of the surface and the OH group; whereas, LUMO, LUMO+1, LUMO+2 are associated mainly with s and p orbitals of In atoms of the cluster, s orbitals of O atoms of the cluster, and s orbitals of O of the OH group. Therefore, these transitions redistribute the charge to make the surface coordinately unsaturated In atom neighboring to an OH electron-deficient and the OH species itself electron-rich, leading to a more Lewis acidic and Lewis basic FLP site on the $In_2O_{3-x}(OH)_y$ surface. Furthermore, the TD of the first three absorption bands of the $In_2O_{3-x}(OH)_y$ surface, Figure 6, illustrates that the nature of the S1, S2, and S3 excited states remains delocalized as compared to other defected surfaces, and involves donor and acceptor orbitals on many O and In atoms including the O of the OH group. In fact, the charge is well delocalized over half of the cluster atoms which contribute significantly to each excitation similar to the case of the pristine surface. This favors easy electron transport on the $In_2O_{3-x}(OH)_y$ surface for the CO_2 reduction reaction, in contrast to the In_2O_{3-x} and $In_2O_3(OH)_y$ surfaces and therefore could explain why CO_2 reduction is favored on the $In_2O_{3-x}(OH)_y$ surface.

These charge analyses also show that the substantial OH character is present in the HOMO of $In_2O_{3-x}(OH)_y$ but is absent in the LUMO. This means that in the presence of light, electrons are transferred from OH to In for the less intense, S0 → S1 transition. In other words, if we consider OH groups behaving as ligands, charge transfer on the $In_2O_{3-x}(OH)_y$ surface has ligand-to-metal charge-transfer (LMCT) character associated with the S0 → S1 transition, in addition to the metal-to-ligand charge-transfer (MLCT) character arising from the S0 → S2 and S0 → S3 transitions. Furthermore, since the oscillator strengths of S0 → S2 and S0 → S3 transitions due to MLCT is more intense than S0 → S1 transition due to LMCT, there will be an overall increase in electronic charge on OH and a decrease in electronic charge on the coordinatively unsaturated surface In atom. Thus, as illustrated in Figure 7,

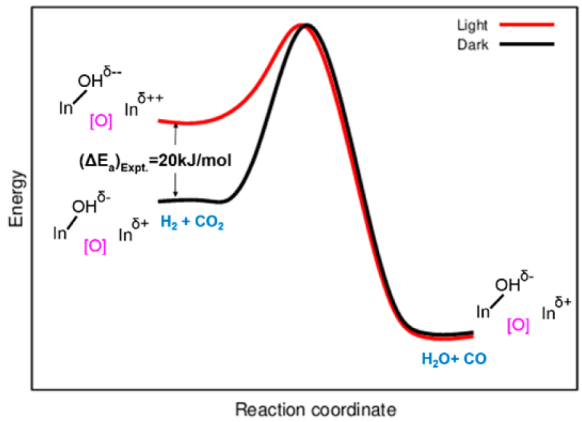

Figure 7. Schematic illustration of the origin of the difference in the experimental activation energy $(\Delta E_a)_{Expt.}$ for the reverse water gas shift reaction $CO_2 + H_2 \rightarrow CO + H_2O$ involving the GS surface FLP in the dark and ES surface FLP in the light. The computational analyses of the GS and ES of the $In_2O_{3-x}(OH)_y$ cluster model showed that the electrons and holes trapped at the Lewis base and Lewis acid sites of the ES surface FLP, enhance their Lewis basicity and Lewis acidity compared to the GS FLP. This increased "frustration of charges" at the surface Lewis pair, consequently decreases the activation barrier for the overall CO_2 reduction reaction, which is supported by the experimental measurements.

in the presence of light, the $In_2O_{3-x}(OH)_y$ surface becomes photoactive due to charge delocalization that enhances the Lewis acidic and Lewis basic character of In···InOH surface FLPs. This highly active excited state FLP surface destabilizes the reactant state and raises its total energy, which could explain the experimentally observed decrease in the activation barrier of CO_2 reduction by 20 kJ mol^{-1} in the light compared to the dark.[10]

■ CONCLUSIONS

For the first time, detailed excited-state calculations have been performed on pristine In_2O_3 and defected In_2O_{3-x}, $In_2O_3(OH)_y$ and $In_2O_{3-x}(OH)_y$ surfaces containing oxygen vacancies and/or hydroxide groups. This has helped to deepen our understanding of the origin of the enhanced CO_2 reduction rate observed for the defected $In_2O_{3-x}(OH)_y$ surface in the light as compared to the dark. All calculations are performed by using

DOI: 10.1021/jacs.5b10179
J. Am. Chem. Soc. 2016, 138, 1206−1214

cluster models saturated with pseudo hydrogens that are found to describe the absorption spectra and electronic properties in good agreement with experimental observations. Our TDDFT calculations show that low energy midgap states are present in absorption spectra for the defected surfaces. It was found that in the presence of O vacancies and surface hydroxyls in the $In_2O_{3-x}(OH)_y$ surface, the lowest energy midgap states exist around 1.5 eV above the VBM, with an oscillator strength of 0.133. This might be due to the unique structural arrangement of atoms within the $In_2O_{3-x}(OH)_y$ surface, which remains more-or-less unchanged upon photoexcitation. Such behavior was not found to occur for the other defected surfaces containing only O vacancies or only hydroxides. Transient absorption spectroscopy and photoconductivity measurements successfully validated the TDDFT computed absorption spectra of $In_2O_{3-x}(OH)_y$ and confirmed the existence of visible and near-infrared transitions associated with midgap states created by the inclusion of O vacancy and OH defects within the cluster. From the molecular orbital and the transition density analyses of the embedded cluster models, the importance of the O vacancy and OH defects in excited state transitions was revealed. These analyses showed that these light-induced electronic transitions were delocalized on In and O atoms for both pristine In_2O_3 and defected $In_2O_{3-x}(OH)_y$ surfaces, whereas for defected In_2O_{3-x} and $In_2O_3(OH)_y$ surfaces, they were localized over their respective defects. In particular, it was found that the population of low lying energy states associated with the $In_2O_{3-x}(OH)_y$ surface enhance the Lewis acidic and Lewis basic character respectively of coordinately unsaturated proximal In and InOH surface FLP sites, which provides the fundamental reason behind the experimentally observed reduction in the activation barrier by about 20 kJ/mol for the gas-phase reaction of H_2 and CO_2 to form CO and H_2O in the presence of light compared to the dark.

■ ASSOCIATED CONTENT

Supporting Information

The Supporting Information is available free of charge on the ACS Publications website at DOI: 10.1021/jacs.5b10179.

Cluster model, diffraction pattern for experimental sample and validation of theoretical model. (PDF)

■ AUTHOR INFORMATION

Corresponding Authors

*gozin@chem.utoronto.ca

*chandraveer.singh@utoronto.ca

Notes

The authors declare no competing financial interest.

■ ACKNOWLEDGMENTS

Financial support for this work was provided by the Ontario Ministry of Research Innovation (MRI); Ministry of Economic Development, Employment and Infrastructure (MEDI); the Natural Sciences and Engineering Research Council of Canada (NSERC), and the Connaught Fund. Computations were performed on the HPC supercomputer at the SciNet HPC Consortium[47] and Calcul Quebec/Compute Canada. SciNet is funded by the Canada Foundation for Innovation under the auspices of Compute Canada, the Government of Ontario, the Ontario Research Fund – Research Excellence, and the University of Toronto. CVS gratefully acknowledges the continued support of the above organizations. GAO is a Government of Canada Research Chair in Materials Chemistry and Nanochemistry. PS and MAE acknowledge the funding from the U.S. National Science Foundation, Division of Chemistry, grant number 1306269. Critical appraisal of this manuscript by Prof. Aron Walsh, Dr. Keith Butler and Dr. Christopher H. Hendon are also deeply appreciated.

■ REFERENCES

(1) Granqvist, C. G.; Hultaker, A. *Thin Solid Films* **2002**, *411*, 1.

(2) Granqvist, C. G. Society of Vacuum Coaters, 50th Annual Technical Conference Proceedings, 2007, 561.

(3) Hamberg, I.; Granqvist, C. G. *J. Appl. Phys.* **1986**, *60*, R123.

(4) Ohta, H.; Orita, M.; Hirano, M.; Hosono, H. *J. Appl. Phys.* **2002**, *91*, 3547.

(5) Yamaura, H.; Jinkawa, T.; Tamaki, J.; Moriya, K.; Miura, N.; Yamazoe, N. *Sens. Actuators, B* **1996**, *36*, 325.

(6) Lorenz, H.; Jochum, W.; Klötzer, B.; Stöger-Pollach, M.; Schwarz, S.; Pfaller, K.; Penner, S. *Appl. Catal., A* **2008**, *347*, 34.

(7) Sato, S. *J. Photochem. Photobiol., A* **1998**, *45*, 361.

(8) Poznyak, S. K.; Golubev, A. N.; Kulak, A. I. *Surf. Sci.* **2000**, *396*, 454.

(9) Bielz, T.; Lorenz, H.; Jochum, W.; Kaindl, R.; Klauser, F.; Klötzer, B.; Penner, S. *J. Phys. Chem. C* **2010**, *114*, 9022.

(10) Ghuman, K. K.; Wood, T. E.; Hoch, L. B.; Mims, C. A.; Ozin, G. A.; Singh, C. V. *Phys. Chem. Chem. Phys.* **2015**, *17*, 14623.

(11) Stephan, D. W. *Acc. Chem. Res.* **2015**, *48*, 306.

(12) Stephan, D. W. *J. Am. Chem. Soc.* **2015**, *137*, 10018.

(13) Stephan, D. W.; Erker, G. *Angew. Chem., Int. Ed.* **2015**, *54*, 6400.

(14) Valiev, M.; Bylaska, E. J.; Govind, N.; Kowalski, K.; Straatsma, T. P.; Van Dam, H. J. J.; Wang, D.; Nieplocha, J.; Apra, E.; Windus, T. L.; Jong, W. A. D. *Comput. Phys. Commun.* **2010**, *181*, 1477.

(15) Govind, N.; Lopata, K.; Rousseau, R.; Andersen, A.; Kowalski, K. *J. Phys. Chem. Lett.* **2011**, *2*, 2696.

(16) Daku, L. M.; Linares, J.; Boillot, M. L. *Phys. Chem. Chem. Phys.* **2010**, *12*, 6107.

(17) Mukhopadhyay, S.; Gowtham, S.; Pandey, R.; Costales, A. *J. Mol. Struct.: THEOCHEM* **2010**, *948*, 31.

(18) Hoch, L. B.; Wood, T. E.; O'Brien, P. G.; Liao, K.; Reyes, L. M.; Mims, C. A.; Ozin, G. A. *Adv. Sci.* **2014**, *1*, 1400013.

(19) Lòpez, R.; Gòmez, R. *J. Sol-Gel Sci. Technol.* **2012**, *61*, 1.

(20) Skinner, D. R.; Whitcher, R. E. *J. Phys. E: Sci. Instrum.* **1972**, *5*, 237.

(21) Casarin, M.; Maccato, C.; Vittadini, A. *Appl. Surf. Sci.* **1999**, *142*, 196.

(22) Casarin, M.; Vittadini, A. *Phys. Chem. Chem. Phys.* **2003**, *5*, 2461.

(23) Casarin, M.; Maccato, C.; Vittadini, A. *J. Phys. Chem. B* **1998**, *102*, 10745.

(24) Sushko, M. L.; Gal, A. Y.; Shluger, A. L. *J. Phys. Chem. B* **2006**, *110*, 4853.

(25) Casarin, M.; Tondello, E.; Vittadini, A. *Surf. Sci.* **1994**, *303*, 125.

(26) Casarin, M.; Giancarlo, F.; Tondello, E.; Vittadini, A. *Surf. Sci.* **1994**, *317*, 422.

(27) Kolczewski, C.; Hermann, K. *Surf. Sci.* **2004**, *552*, 98.

(28) Zhang, K. H. L.; Walsh, A.; Catlow, C. R. A.; Lazarov, V. K.; Egdell, R. G. *Nano Lett.* **2010**, *10*, 3740.

(29) Lany, S.; Zakutayev, A.; Mason, T. O.; Wager, J. F.; Poeppelmeier, K. R.; Perkins, J. D.; Berry, J. J.; Ginley, D. S.; Zunger, A. *Phys. Rev. Lett.* **2012**, *108*, 016802.

(30) Lei, F.; Sun, Y.; Liu, K.; Gao, S.; Liang, L.; Pan, B.; Xie, Y. *J. Am. Chem. Soc.* **2014**, *136*, 6826.

(31) Atkins, P. W. *Molecular Quantum Mechanics*, 2nd ed.; W. H. Freeman and Company: San Francisco, CA, 1982; pp 201–202.

(32) Zhang, J. Z. *J. Phys. Chem. B* **2000**, *104*, 7239.

(33) Triggiani, L.; Brunetti, A.; Aloi, A.; Comparelli, R.; Curri, M. L.; Agostiano, A.; Striccoli, M.; Tommasi, R. *J. Phys. Chem. C* **2014**, *118*, 25215.

(34) Yang, X.; Tamai, N. *Phys. Chem. Chem. Phys.* **2001**, *3*, 3393.

DOI: 10.1021/jacs.5b10179
J. Am. Chem. Soc. 2016, 138, 1206–1214

(35) Othonos, A.; Zervos, M.; Tsokkou, D. *Nanoscale Res. Lett.* **2009**, *4*, 526.
(36) Ruckebusch, C.; Sliwa, M.; Pernot, P.; Juan, A. D.; Tauler, R. *J. Photochem. Photobiol., C* **2012**, *13*, 1.
(37) Berera, R.; Grondelle, R. V.; Kennis, J. T. M. *Photosynth. Res.* **2009**, *101*, 105.
(38) Zhao, H.; Zhang, Q.; Weng, Y.-X. *J. Phys. Chem. C* **2007**, *111*, 3762.
(39) Yoshihara, T.; Katoh, R.; Furube, A.; Tamaki, Y.; Murai, M.; Hara, K.; Murata, S.; Arakawa, H.; Tachiya, M. *J. Phys. Chem. B* **2004**, *108*, 3817.
(40) Katoh, R.; Murai, M.; Furube, A. *Chem. Phys. Lett.* **2010**, *500*, 309.
(41) Yamamoto, T.; Ohno, T. *Phys. Chem. Chem. Phys.* **2012**, *14*, 589.
(42) Ahmed, S. M.; Szymanski, P.; El-Nadi, L. M.; El-Sayed, M. A. *ACS Appl. Mater. Interfaces* **2014**, *6*, 1765.
(43) Wang, X.; Feng, Z.; Shi, J.; Jia, G.; Shen, S.; Zhou, J.; Li, C. *Phys. Chem. Chem. Phys.* **2010**, *12*, 7083.
(44) Blood, P.; Orton, J. W. *The Electrical Characterization of Semiconductors: Majority Carriers and Electron States*; Academic Press: 1992; Chapter 13.
(45) Nagpal, P.; Klimov, V. I. *Nat. Commun.* **2011**, *2*, 486.
(46) Walsh, A.; Catlow, C. R. A. *J. Mater. Chem.* **2010**, *20*, 10438.
(47) Loken, C.; Gruner, D.; Groer, L.; Peltier, R.; Bunn, N.; Craig, M.; Henriques, T.; Dempsey, J.; Yu, C.-H.; Chen, J.; Dursi, L. J.; Chong, J.; Northrup, S.; Pinto, J.; Knecht, N.; Zon, R. V. *J. Phys. Conf. Ser.* **2010**, *256*, 012026.

DOI: 10.1021/jacs.5b10179
J. Am. Chem. Soc. 2016, 138, 1206−1214